ORIGINAL ARTICLE

Anatomical and electrophysiological changes in striatal TH interneurons after loss of the nigrostriatal dopaminergic pathway

Bengi Ünal · Fulva Shah · Janish Kothari ·
James M. Tepper

Abstract Using transgenic mice that express enhanced green fluorescent protein (EGFP) under the control of the tyrosine hydroxylase (TH) promoter, we have previously shown that there are approximately 3,000 striatal EGFP-TH interneurons per hemisphere in mice. Here, we report that striatal TH-EGFP interneurons exhibit a small, transient but significant increase in number after unilateral destruction of the nigrostriatal dopaminergic pathway. The increase in cell number is accompanied by electrophysiological and morphological changes. The intrinsic electrophysiological properties of EGFP-TH interneurons ipsilateral to 6-OHDA lesion were similar to those originally reported in intact mice except for a significant reduction in the duration of a characteristic depolarization induced plateau potential. There was a significant change in the distribution of the four previously described electrophysiologically distinct subtypes of striatal TH interneurons. There was a concomitant increase in the frequency of both spontaneous excitatory and inhibitory post-synaptic currents, while their amplitudes did not change. Nigrostriatal lesions did not affect somatic size or dendritic length or branching, but resulted in an increase in the density of proximal dendritic spines and spine-like appendages in EGFP-TH interneurons. The changes indicate that electrophysiology properties and morphology of striatal EGFP-TH interneurons depend on endogenous levels of dopamine arising from the nigrostriatal pathway. Furthermore, these changes may serve to help compensate for the changes in activity of spiny projection neurons that occur following loss of the nigrostriatal innervation in experimental or in early idiopathic Parkinson's disease by increasing feedforward GABAergic inhibition exerted by these interneurons.

Introduction

The neostriatum is the main point of entry within the basal ganglia for excitatory inputs arising from the cortex and the thalamus. Recent findings reveal that interaction between striatal interneurons and spiny projection neurons (SPNs) plays an essential role in shaping striatal output (Koós and Tepper 1999; Koós et al. 2004; Tepper and Bolam 2004; Gittis et al. 2010; English et al. 2011). Striatal interneurons make up only about 5 % of the striatal cell population in rodents (Wilson and Kawaguchi 1996; Rymar et al. 2004) but manifest great electrophysiological, neurochemical and morphological diversity. Striatal interneurons can be classified as either cholinergic or GABAergic. Striatal GABAergic interneurons can be further subdivided into parvalbumin-expressing (PV) fast-spiking (FSI), neuropeptide Y-expressing (NPY) persistent low-threshold spiking (PLTS), NPY+ neurogliaform (NPY-NGF) or calretinin-expressing (CR) interneurons (Kawaguchi 1993, 1997; Wu and Parent 2000; Tepper and Bolam 2004; Tepper et al. 2010; Ibanez-Sandoval et al. 2011). Using bacterial artificial chromosome (BAC) transgenic mice that express enhanced green fluorescent protein (EGFP) under the control of the tyrosine hydroxylase (TH) promoter (EGFP-TH mice), we have shown that striatal TH neurons

B. Ünal · F. Shah · J. Kothari · J. M. Tepper (✉)
Center for Molecular and Behavioral Neuroscience, Aidekman Research Center, Rutgers University, 197 University Avenue, Newark, NJ 07102, USA
e-mail: jtepper@andromeda.rutgers.edu

comprise four distinct groups of GABAergic interneurons, Types I to IV, based on passive and active membrane properties and neurocytology (Ibáñez-Sandoval et al. 2010).

Since their initial discovery in primate striatum (Dubach et al. 1987), striatal TH neurons have sparked a great deal of interest; TH is the rate-limiting enzyme in dopamine (DA) synthesis and is the most commonly used marker used to identify the dopaminergic phenotype in substantia nigra (SN) and ventral tegmental area neurons (VTA) (e.g., Ungless et al. 2004; Henny et al. 2012 but see also Ugrumov 2009). Consequently, a number of studies have investigated the developmental and molecular origin of striatal TH neurons (Busceti et al. 2008, 2012) and their fate in animal models of Parkinson's disease (PD) and/or in human idiopathic PD. It is generally acknowledged that there is a marked (200–400 %) increase in the number striatal TH neurons following lesions of the nigrostriatal pathway (Tashiro et al. 1989; Betarbet et al. 1997; Meredith et al. 1999; Porritt et al. 2000; Palfi et al. 2002; Mazloom and Smith 2006; Huot and Parent 2007; Tandé et al. 2006; Huot et al. 2007). Since a possible role of neurogenesis in the appearance of these neurons has been ruled out by nucleotide uptake studies (e.g., Darmopil et al. 2008; Tandé et al. 2006), the most widely accepted explanation for the increase in striatal TH neurons is a compensatory phenotypic conversion of a population of pre-existing striatal neurons.

However, there remains uncertainty as to the origin of the "new" striatal TH interneurons after dopamine depletion, and there has been no attempt at electrophysiological characterization of striatal TH neurons following lesions of the nigrostriatal pathway. Similarly, the identification of the "new" TH-expressing neurons appearing after DA depleting lesions as spiny projections neurons or striatal interneurons remains controversial (e.g., Darmopil et al. 2008; Ibáñez-Sandoval et al. 2010; Masuda et al. 2011).

To resolve these outstanding questions we employed the same BAC EGFP-TH mice used previously (Ibáñez-Sandoval et al. 2010; Ünal et al. 2011) to determine the effects of unilateral 6-hydroxydopamine (6-OHDA) lesion of the nigrostriatal pathway on the number, and physiological and morphological characteristics of striatal EGFP-TH interneurons.

Methods

Subjects

The progeny of hemizygous BAC transgenic mice Tg(Th-EGFP)DJ76Gsat/Mmnc (GENSAT, http://www.mmrrc. org/strains/292/0292.html) obtained from the Mutant Mouse Regional Resource Center at University of North Carolina, Chapel Hill and crossed to wild type FVB mice were used in the experiments. Mice of both sexes between 2 and 10 months were used in all experiments. The animals were kept in a temperature and humidity controlled AA-ALAC accredited animal facility and maintained on a 12/12 h dark/light cycle with light onset at 7 am. Prior to experiments, mice were genotyped from tail snips to confirm that they expressed EGFP. All experimental protocols were in accordance with the Rutgers University Institutional Animal Care and Use Committee and the NIH Guidelines to the Care and Use of Laboratory Animals. Utmost effort was shown to minimize the number of animals used and any discomfort the animals underwent. A total of 86 mice were used in these experiments.

6-OHDA lesions

Under isoflurane anesthesia, mice were fixed in a stereotaxic apparatus (Kopf Instruments). After a subcutaneous injection of bupivacaine (0.5 %, Henry Schein, Melville, NY, USA), an incision was made on the scalp. Following anterior–posterior and medio-lateral flat skull adjustments, a small burr hole was drilled on the skull overlying SN unilaterally (3.4 mm posterior and 1.0 mm lateral with respect to bregma) (Franklin and Paxinos 2007). Mice received desipramine (Sigma-Aldrich, St. Louis, MO; 25 mg/kg) i.p. 30 min prior to 6-OHDA infusions to prevent the uptake of toxin by noradrenergic terminals (Breese and Traylor 1971). A glass micropipette (50 μm o.d. tip) was filled with freshly prepared 6-OHDA-HCl (Sigma-Aldrich, St. Louis, MO, USA, 3.6 μg/μl 6-OHDA in 0.9 % sterile saline containing 0.2 % ascorbate) or vehicle. 6-OHDA (1.8 μg/0.5 μl) or vehicle (0.5 μl) was pressure injected over 15 min unilaterally into the right or left SN pars compacta (SNc) (4.3 mm ventral from the dura) in a counterbalanced fashion. Upon completion of injections, the glass capillaries were left in place for 3 additional minutes to allow diffusion before being slowly retracted. The scalp was sutured with 4–0 surgical silk and the wound was infiltrated with bupivacaine and bacitracin ointment. Lactated Ringer's solution (1 ml) and buprenorphine (0.05 mg/kg) were administered s.c. and mice allowed to recover under a heat lamp, returned to home cages, and kept there until use. The weight of the mice, and their food and water intake was monitored post-surgically and where needed, mice were provided with 10 % sucrose solution and non-sweetened cereal pieces during recovery.

To evaluate the extent of the unilateral 6-OHDA lesion, EGFP-TH neurons in SNc and VTA were counted in 6-OHDA and vehicle-treated hemispheres in 60 μm coronal midbrain sections taken from 3.3 to 3.5 mm posterior to

bregma. The degree of loss of EGFP-TH neurons in SNc and VTA was determined by dividing the numbers from the 6-OHDA-treated side by the numbers from the vehicle-treated side for SNc and VTA. In addition, forelimb use asymmetry was assessed using a cylinder test as described in Cenci and Lundblad (2007) prior to euthanasia. Mice were initially habituated to the experimental room for 5 min prior to behavioral phenotyping. Mice were placed inside a glass cylinder of 10 cm in diameter and 12 cm in height in a dimly lit room. Behaviors were recorded for 3 min with a digital camera. Behavioral sessions were analyzed offline frame-by-frame. For behavioral scoring, forelimb use asymmetry was calculated by dividing the total sum of contralateral front paw placements on the cylinder wall by the total sum of ipsi- and contralateral paw placements for each mouse. 40 % was regarded as a cutoff value, indicating the success of the lesion.

Retrograde labeling

In a subgroup of unilaterally 6-OHDA-lesioned mice ($n = 5$), 0.1 μl of rhodamine microspheres (Lumafluor, Durham, NC) was pressure injected (Picospritzer, Intracel Ltd., UK) over 15 min bilaterally into the globus pallidus external segment (GPe) (0.4 mm posterior and 1.7 mm lateral with respect to bregma and 3.5 mm ventral from the dura) and substantia nigra pars reticulata (SNr) (3.4 mm posterior and 1.4 mm lateral with respect to bregma and 4.5 mm ventral from the dura) to determine whether any of the EGFP-TH neurons were projection neurons. Mice were sacrificed at 3, 7, 14 or 28 days post-lesion following deep anesthesia with i.p. ketamine/xylazine (160/30 mg/kg) and transcardially perfused with chilled Ringer's solution followed by 4 % paraformaldehyde in 0.1 M PB. Brains were post-fixed overnight at 4 °C and were subsequently transferred into 30 % sucrose in 0.1 M PB. Sixty micrometer coronal sections containing the striatum and the injection sites were cut on a freezing microtome (Microm, Heidelberg, Germany) and mounted on glass slides in Vectashield HardSet mounting medium (Vector Laboratories, Burlingame, CA) and coverslipped. Sections were analyzed for co-localization of EGFP-TH and rhodamine with an Olympus BX51 epifluorescence microscope.

Cell counting

A separate group of EGFP-TH mice ($n = 16$) underwent the same 6-OHDA lesioning procedures described above and was sacrificed at 3, 7, 14 or 28 days post-injection. Coronal striatal sections were prepared as described above. Unbiased cell counting was done using the optical fractionator probe of StereoInvestigator (Microbrightfield v.10, Burlingame, VT). Briefly, after randomly determining the

starting section for each series, the contour of every fifth section was traced at 4×. Then a 544 × 380 μm grid was overlaid on the contoured serial sections and cell counting of fluorescent striatal EGFP-TH somata was performed at 40× under 380 nm epifluorescence illumination. Disector frame dimensions were set to 180 × 180 μm with 30 μm z depth and 5 % guard zones on top and at the bottom. Only whole EGFP-TH somata falling within the borders or coming in contact with inclusion borders but not touching the exclusion borders were counted.

In mice that also had bilateral rhodamine bead injections into GPe and SNr, striatal EGFP-TH somata were further investigated for co-localization of retrogradely transported rhodamine microspheres under epifluorescence illumination at 530 nm. These data were used to estimate the total number of EGFP-TH-only neurons and double-labeled EGFP-TH/rhodamine + neurons in striatum.

Immunocytochemistry

Briefly, 60 μm coronal sections from 3 to 7 days post-6-OHDA-lesioned mice were pretreated with 1 % sodium borohydride followed by 10 % methanol and 3 % H_2O_2 in PBS. Sections were then incubated in 10 % normal donkey serum, 2 % bovine serum albumin and 0.5 % Triton X-100 for 1 h. Alternating serial sections were incubated with one of the following primary antibodies for 48 h at 4 °C: rabbit anti-TH (1:1,500, Millipore Cat. #: AB9983), rabbit anti-PV (1:1,000, Immunostar Cat. #24428), rabbit anti-NPY (1:3,000, Immunostar Cat. #: 22940), rabbit anti-CR (1:1,500; Millipore Cat. #: AB5054), goat anti-choline acetyl transferase (1:400, Millipore Cat. #: AB144). After rinsing 3 times for 10 min in PBS, sections were transferred into a solution containing 1:200 donkey anti-rabbit Alexa 594 or 1:200 donkey anti-goat Alexa 594 (Molecular Probes, Inc., Eugene, OR, USA, Cat. #'s: A21207 and A11058) in PBS at 4 °C overnight.

Ex vivo electrophysiology

A group of animals that underwent unilateral DA denervation was sacrificed at 3, 7, 14 or 28 days post-lesion. Following euthanasia as described above, EGFP-TH mice were transcardially perfused with ice-cold modified Ringer's solution that contained (in mM) 124 choline chloride, 2.5 KCl, 26 NaHCO$_3$, 3.3 MgCl$_2$, 1.2 NaH$_2$PO$_4$, 10 glucose, 0.5 CaCl$_2$ and 250 μm coronal striatal sections were obtained using a vibrating microtome (Vibrotome^{TM} 3000). Slices were transferred initially into a slice chamber that contained oxygenated Ringer's solution (in mM 124 NaCl, 2.5 KCl, 26 NaHCO$_3$, 1.3 MgCl$_2$, 1.2 NaH$_2$PO$_4$, 10 glucose, 2 CaCl$_2$, 1 ascorbic acid, 3 pyruvate, 0.4 myoinositol) maintained at 33 °C and later kept at room temperature

until the time of recording. During the recordings, slices were continuously perfused with normal oxygenated Ringer's solution at a flow rate of 2 ml/min that was maintained at 33 °C via a TC-324B inline heater system (Warner Instruments, Hamden, CT). EGFP-TH neurons throughout striatum were identified under epifluorescence illumination and then patched under infrared DIC using a BX50-WI Olympus epifluorescence microscope with a 40× water immersion objective. Whole-cell current clamp recordings were obtained with 1.5 mm glass micropipettes (Harvard Apparatus), 3–7 MΩ resistance fabricated on a two-stage vertical puller (Narishige, PP-83). Current clamp recordings were obtained with an internal solution containing (in mM): 130 KMeSO$_3$, 10 NaCl, 10 HEPES, 1 EGTA, 0.1 CaCl$_2$, 2 MgCl$_2$, 3 ATP, 0.3 GTP, pH adjusted to 7.3. Biocytin (0.2 %) was added to the intracellular solution for subsequent identification, reconstruction and morphological analysis of recorded striatal EGFP-TH neurons.

For recording spontaneous synaptic events in voltage clamp, a cesium-based internal solution was used that contained (in mM) (Mathus et al. 2011): 120 CsMeSO$_4$, 5 NaCl, 10 TAE-Cl, 10 HEPES, 5 QX-314, 1.1 EGTA, 0.3 Na-GTP and 4 Mg-ATP which was adjusted to pH 7.3 with CsOH. Spontaneous excitatory synaptic currents were isolated by holding the cell at −70 mV in the presence of bicuculline methiodide (10 μM, Sigma). Spontaneous inhibitory synaptic currents were isolated by holding the cell at 0 mV in the presence of AP-5 (25 μM, Tocris) and CNQX (10 μM, Tocris).

Data were acquired with a Neurodata IR-283 for current clamp or with a Multiclamp 700B (Molecular Devices) for current clamp and voltage-clamp recordings. Data were digitized at 10–40 kHz via a Micro 1401 Mk II digitizer and transferred to a PC running Signal v.4 software (CED, Cambridge, UK) for offline analysis.

Electrophysiological data were analyzed using CED Signal and spontaneous synaptic events were analyzed using Clampfit (v.10; Axon Instruments) using template-based event detection. To obtain the basic electrophysiological parameters of the EGFP-TH neurons, a sequence of hyperpolarizing and depolarizing 500 ms current steps ranging from −200 pA to +200 pA with 20 pA increments were injected at 0.2 Hz. Current (I) voltage (V) curves were constructed by averaging 10 ms portion of a 500 ms subthreshold current injection step that were devoid of spontaneous synaptic potentials. Membrane input resistance was estimated from the slope of the IV curve at the resting membrane potential. Action potential (AP) measurements were taken from the first AP evoked by injection of threshold depolarizing current. AP threshold was determined as the point at which slope of voltage rise reached 10 mV/msec. AP amplitude was defined as the voltage difference between AP

threshold and the peak. AP duration was determined by measuring the time between points at half-maximal action potential amplitude. Spike after hyperpolarization (AHP) amplitude was measured by subtracting the voltage minimum following the first evoked AP from the AP threshold value. The membrane time constant (τ) was calculated by fitting a single exponential to the initial phase of the membrane response to −20 pA current pulse. As reported previously (Ibáñez-Sandoval et al. 2010), some EGFP-TH cells exhibited a membrane voltage sag in response to hyperpolarizing current injections. We quantified a sag ratio by dividing the maximum hyperpolarization by steady state membrane potential at the end of the 500 ms pulse when cells were hyperpolarized to −100 mV. Maximal firing rate was measured by 1/first interspike interval (ISI) during a +200 pA current pulse. We also measured spike frequency adaptation in the first trace in which three or more spikes were elicited by current injection by dividing the last ISI by the first ISI. In addition, we quantified the amplitude and duration of the plateau potentials emerging at the offset of 0.5 s of +100 pA depolarizing current by fitting a Boltzmann sigmoid $y = (A_1 - A_2)/\left(1 + e^{(x - x_{50})/dx}\right) + A_2$, where the difference between A_1 and A_2 was used to measure plateau potential amplitude and x_{50} was used to determine the time when plateau potential decays to half-maximal level.

In voltage-clamp recordings where we used a cesium-based intracellular solution, we compared amplitude, rise and decay time constants, inter-event intervals (IEI), coefficient of variation of IEIs and frequency of pharmacologically isolated spontaneous excitatory (sEPSC) and inhibitory post-synaptic currents (sIPSC) from 1 min epochs of recordings from neurons clamped at −70 and 0 mV holding potentials, respectively.

Biocytin cytochemistry and cell reconstruction

Following electrophysiological characterization, sections containing biocytin-filled neurons were fixed in 4 % paraformaldehyde in 0.1 M PB overnight at 4 °C and transferred into 0.1 M PB. Sections were washed for 3 × 10 min in 0.1 M PB followed by 10 % methanol and 3 % H$_2$O$_2$ for 15 min, and incubated with avidin–biotin-peroxidase complex (vector laboratories; 1:200) in 0.1 % Triton X-100 overnight at 4 °C. After washing 6 times for 10 min in 0.1 M PB, the sections were reacted with 3,3′-diaminobenzidine (0.025 %) and H$_2$O$_2$ (0.0008 %) in 0.1 M PB with nickel intensification (2.5 mM nickel ammonium sulfate and 7 mM ammonium chloride) to visualize the biocytin-stained neuron. Sections were air dried on gelatin coated slides and coverslipped in Depex (EMS, Harfield, PA). A subset of these sections (3 from 6-OHDA- and 3 from vehicle-treated striata) were later

post-fixed in osmium tetroxide (0.1 % in PB) for 30 min, dehydrated through a graded series of ethanol and three additional 10 min washes with propylene oxide and then cured with Fluka Durcupan resin (EMS, Hatfield PA) for 1 day at room temperature then at 60 °C for 3 days.

For three-dimensional reconstructions of biocytin-injected neurons, stacks of images were taken with a 60× or 100× oil immersion lens with an Olympus BX51 microscope using Neurolucida (v.10, MBF Biosciences, VT). Neurons were manually traced from virtual image stacks with Neurolucida (v.10). Morphometry and Sholl analyses (Sholl 1953) were done on the reconstructions with Neurolucida Explorer by taking the soma as the center and then superimposing regularly spaced (10 μm) concentric spheres on the neurites to calculate the number of intersections and measure dendritic length and number of dendritic spines per shell.

Statistics

Data were analyzed with the IBM SPSS Statistics package (v.20). Cell count data comparisons were done between 6-OHDA- and vehicle-treated striata, therefore, a paired t test was used. Student's two-tailed t test and multivariate ANOVA (MANOVA) were used for appropriate data sets. In cases where homogeneity of variance could not be assumed, Chi-Square, Mann–Whitney and Kruskal–Wallis tests were used as appropriate. Significance level was set at 0.05.

Results

Unilateral 6-OHDA lesion: immunocytochemical and behavioral characterization of lesion extent

Unilateral intranigral infusion of 6-OHDA resulted in a profound loss of EGFP-TH expressing and TH immuno-reactive somata and neurites in the central and lateral segments of substantia nigra at all time points sampled, whereas the most medial aspects of SN and the VTA were spared (Fig. 1a–c). Vehicle infusion into the contralateral SN did not lead to any loss of EGFP-TH or TH immuno-fluorescence. In the SNc, the average loss of dopaminergic cells was 85 ± 3.3 % where in VTA it was 54 ± 7.8 %. There was no significant effect of time (3, 7, 14 or 28 days) on the average loss of EGFP-TH cells in SNc or VTA (χ^2 (8, 3), $p = 0.884$ and $p = 0.212$, respectively).

Loss of inherent EGFP-TH signal and TH immunoflu-orescence was clearly evident in dorsal striatum ipsilateral to the intranigral 6-OHDA infusion (Fig. 1d–f). Some TH-expressing fibers remained in the ventral striatum (Fig. 1e). The contralateral striatum demonstrated strong EGFP-TH

expression and TH-immunolabeling. Of particular interest, in the lesioned striatum, several (18 %; 17 out of 97 ste-reologically sampled) EGFP-TH somata were found to co-localize TH immunofluorescence. One example is shown in Fig. 1g–i. This is in contrast to the case in normal striatum where TH immunoreactivity is generally not seen in EGFP-TH neurons unless the mice have been treated with col-chicine to block axonal transport and increase somatic levels of the protein (Ibáñez-Sandoval et al. 2010). The presence of co-localization of TH and EGFP fluorescence after 6-OHDA lesions suggests that the dopamine dener-vation has increased the levels of TH in the striatal TH neurons, presumably by increasing the production of TH.

In a subgroup of unilaterally 6-OHDA-lesioned mice ($n = 11$), offline analysis of behavior in the cylinder test showed a significantly higher number of ipsilateral forepaw contacts with the walls of the cylinder [t (1, 10) = −4.66; $p = 0.001$, data not shown]. The mean front limb asym-metry score and total number of front limb contacts did not differ across different time points post-lesion [χ^2 (12, 3), $p = 0.748$ and $p = 0.350$, respectively].

Effect of 6-OHDA lesion on the number and distribution of striatal EGFP-TH neurons

In the lesioned hemisphere, stereological estimates of striatal EGFP-TH neuron numbers from all time points (3, 7, 14, 24 days post-lesion) ranged from ∼2,100 to 4,500 whereas in the vehicle-treated hemisphere the cell counts ranged from ∼1,800 to 3,500 (Gundersen's coefficient of error = 0.103 ± 0.004). The increase in the total number of striatal (dorsal plus ventral striatum) EGFP-TH neuron ipsilateral to the nigrostriatal lesion was significantly greater than in the contralateral control side [paired t test (13) = 2.94, $p = 0.012$] (Fig. 2a). To take inter-individual variability into account, stereological estimates of EGFP-TH cell counts were normalized across subjects by expressing cell numbers as the percent difference in the cell counts in the ipsilateral hemisphere to the counts obtained from the vehicle-treated hemisphere (Fig. 2b). At 3 days post-injection, the ipsilateral striatum contained 30 % more EGFP-TH neurons than the vehicle-treated hemisphere, a difference that decreased with time (Fig. 2b).

However, when the changes in striatal counts were analyzed after parsing the striatum into dorsal striatal (dSTR) and ventral striatal (vSTR) divisions with a 4 × 2 × 2 MANOVA [days post-injection by striatal division by treatment (6-OHDA vs. vehicle)], the analysis revealed a significant main effect of treatment [F (1, 30) = 6.2, $p = 0.019$]. The three-way interaction among striatal division, days post-injection and treatment was also statistically significant [F (6, 30) = 2.529, $p = 0.042$]. Post hoc tests using LSD indicated that normalized
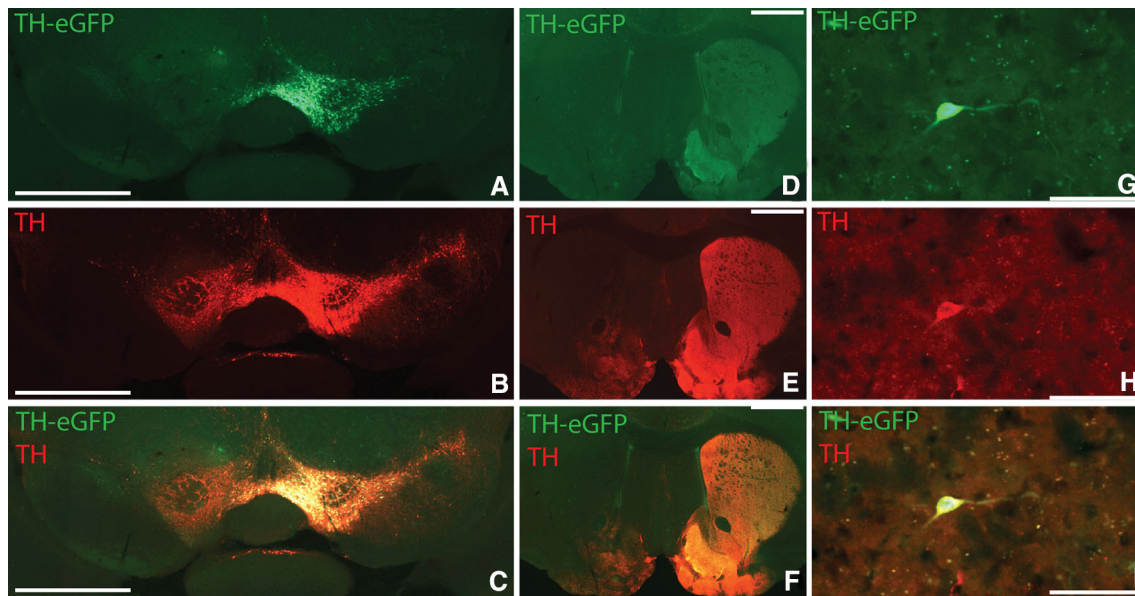
Fig. 1 Fluorescence photomicrographs of EGFP-TH expression (*green*) and TH immunoreactivity (*red*) in substantia nigra and striatum in unilaterally 6-OHDA-treated EGFP-TH mice. Substantial loss of EGFP-TH fluorescence (**a**) and TH immunofluorescence (**b**) was evident in 6-OHDA-treated left SNc whereas neighboring VTA was relatively spared. Vehicle-treated right SNc did not show any discernable loss. The merge of **a** and **b** is shown in **c**. Left striatum ipsilateral to 6-OHDA-treated SNc sustained major loss of EGFP-TH (**d**) and TH. The merge of **d** and **e** is shown in **f**. Representative example of the subset of striatal EGFP-TH (**g**) neurons from 6-OHDA-treated side that co-expressed TH immunofluorescence (**h**, **i**). *Scale bars* 1 mm (**a**–**f**), 50 μm (**g**–**i**)

Fig. 2 Changes in striatal EGFP-TH cell counts following unilateral 6-OHDA lesion. **a** There was a significant increase in stereological estimates of striatal EGFP-TH neuron numbers after 6-OHDA lesion (paired *t* test). **b** Increase in striatal EGFP-TH numbers normalized to vehicle-treated side indicates that overall there was a 30 % increase in the earliest time points (3 and 7 days) but counts decline back to control levels within 2 weeks (MANOVA). **c** Changes in dorsal striatal EGFP-TH numbers normalized to vehicle-treated side (MANOVA). **d** Changes in ventral striatal EGFP-TH numbers normalized to vehicle-treated side (MANOVA)
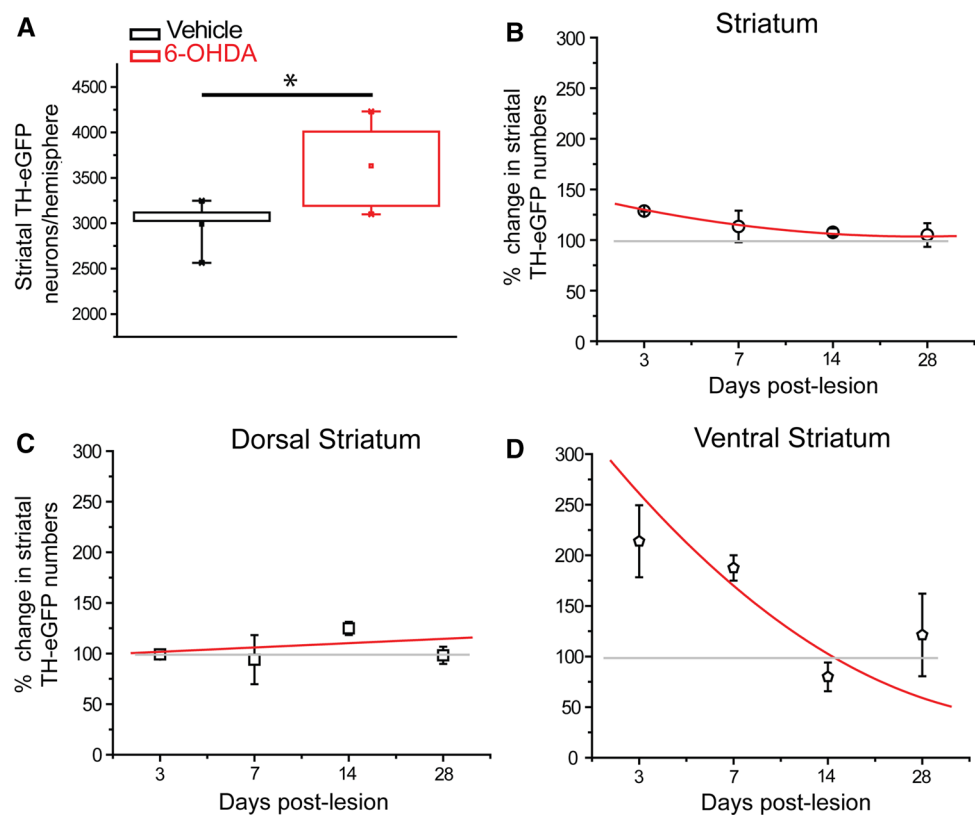
EGFP-TH counts on post-lesion day 3 were significantly higher than at days 14 and 28 ($LSD_{3-14} = 28.1$, $p = 0.037$; $LSD_{3-28} = 30.91$, $p = 0.036$).

Cell counts of EGFP-TH neurons in dorsal striatum as a function of time post-injection did not differ significantly [F (3, 3) = 1.322, $p = 0.412$] (Fig. 1c). However, in ventral striatum, cell counts at different post-lesion time points were significantly different [F (3, 3) = 51.760, $p = 0.004$]. At 3 days post-lesion in the ipsilateral vSTR, EGFP-TH neuron cell counts were 2.1 times greater than counts from the contralateral side, a difference that decreased at subsequent time points (Fig. 2d).

We previously showed that none of the striatal EGFP-TH neurons in normal BAC transgenic mice was retrogradely labeled following large injections of fluorescent beads into substantia nigra and globus pallidus, consistent with electrophysiological and morphological properties indicating that these were interneurons that were completely distinct from spiny projection neurons Ibáñez-Sandoval et al. (2010). However, the possibility remained that some of the EGFP-TH neurons that accounted for the increased number of striatal EGFP-TH neurons that we observed following ipsilateral destruction of the nigrostriatal DA input resulted from a phenotypic shift in which spiny projection neurons might start expressing TH, as suggested elsewhere (e.g., Darmopil et al. 2008). Thus, we repeated the retrograde tracing experiments, making 0.1 μl injections of fluorescent beads into the SN and GP ipsilateral to a nigral 6-OHDA injection in 5 mice. Just as in control mice, none of the striatal EGFP-TH neurons was found to be double labeled in the dorsal striatum or in the ventral striatum (Fig. 3) consistent with our previous claims that all of the striatal EGFP-TH neurons in both lesioned and control striata are, in fact, interneurons.

Effect of 6-OHDA lesion on striatal interneuron neurochemical markers

We previously tested striatal EGFP interneurons for co-localization with PV, NOS and CR in control EGFP-TH mice. No immunoreactivity for any of these substances was observed in EGFP-TH interneurons Ibáñez-Sandoval et al. (2010). However, by the same logic discussed above, the possibility remained that following dopaminergic denervation, a phenotypic shift could occur that would lead to the expression of TH and/or EGFP-TH in other striatal GABAergic interneurons that do not normally express this enzyme.

Therefore, co-localization of EGFP-TH with PV, ChAT, NPY and CR was investigated by immunofluorescence in four unilaterally 6-OHDA-lesioned EGFP-TH mice (3 days to 1 week post-lesion), by random sampling of EGFP-TH neurons using the optical fractionator workflow in StereoInvestigator (v. 10). Out of 159 EGFP-TH
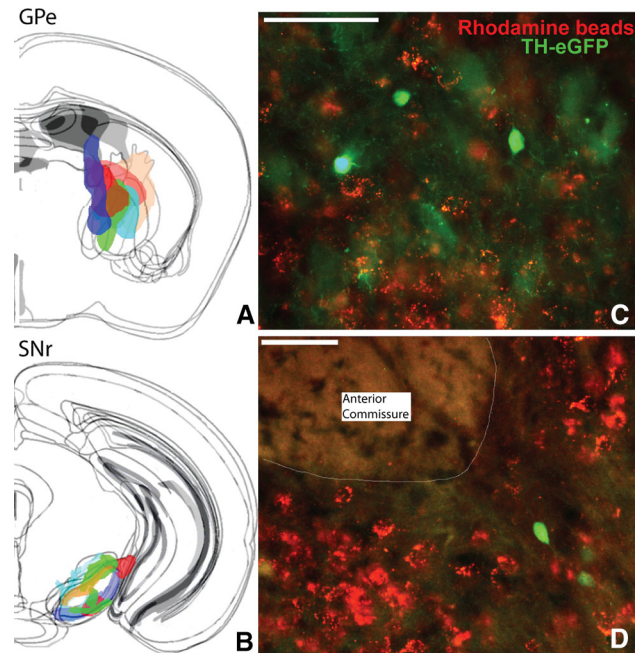
Fig. 3 EGFP-TH interneurons do not project to GPe or SNr. **a** Retrograde label injection sites in GPe are indicated on atlas images, each color corresponds to a separate mouse. **b** Retrograde label injection sites in SNr are indicated on atlas images, each color corresponds to a separate mouse. Lack of retrograde label incorporation in dorsal (**c**) and ventral (**d**) striatal EGFP-TH cells, despite heavy labeling of neighboring neurons. *Scale bars* 50 μm

neurons, none was positive for NPY. In addition, none of the 312 EGFP-TH cells sampled in lesioned and vehicle-treated striatum showed co-localization with ChAT and none of 234 EGFP-TH cells sampled in lesioned or vehicle-treated striatum co-localized PV (Fig. 4). However, 6 EGFP-TH neurons out of 138 sampled cells (2/63 in vehicle treated striatum; 4/75 in 6-OHDA-lesioned striatum) showed co-localization with CR indicating that ~5 % of EGFP-TH cells are CR immunoreactive (Fig. 5). Critically, however, the proportion of EGFP-TH neurons that co-localize CR does not change after DA lesion.

To address the possibility that the increased numbers of striatal EGFP-TH neurons came about from a phenotypic shift in which one or more of the other striatal interneuron subtypes ceased producing their characteristic neurochemical marker, we performed similar stereological cell counts of PV, NPY, CR and ChAT interneurons. There were no changes in the cell counts for any of these striatal interneurons following 6-OHDA lesions as compared to the contralateral side. These results are shown in Table 1.

Overall, these experiments demonstrate that it is highly unlikely that the increase in the number of striatal EGFP-TH interneurons following 6-OHDA lesions of the nigrostriatal pathway result from a phenotypic expression change in either SPN or ChAT, PV, NPY or CR interneurons.

Fig. 4 Comparison of EGFP-TH expression with other striatal interneuronal markers. EGFP-TH cells did not show any overlap with NPY immunoreactivity (**a**), ChAT immunoreactivity (**b**) or with PV immunoreactivity (**c**). *Scale bars* 50 μm
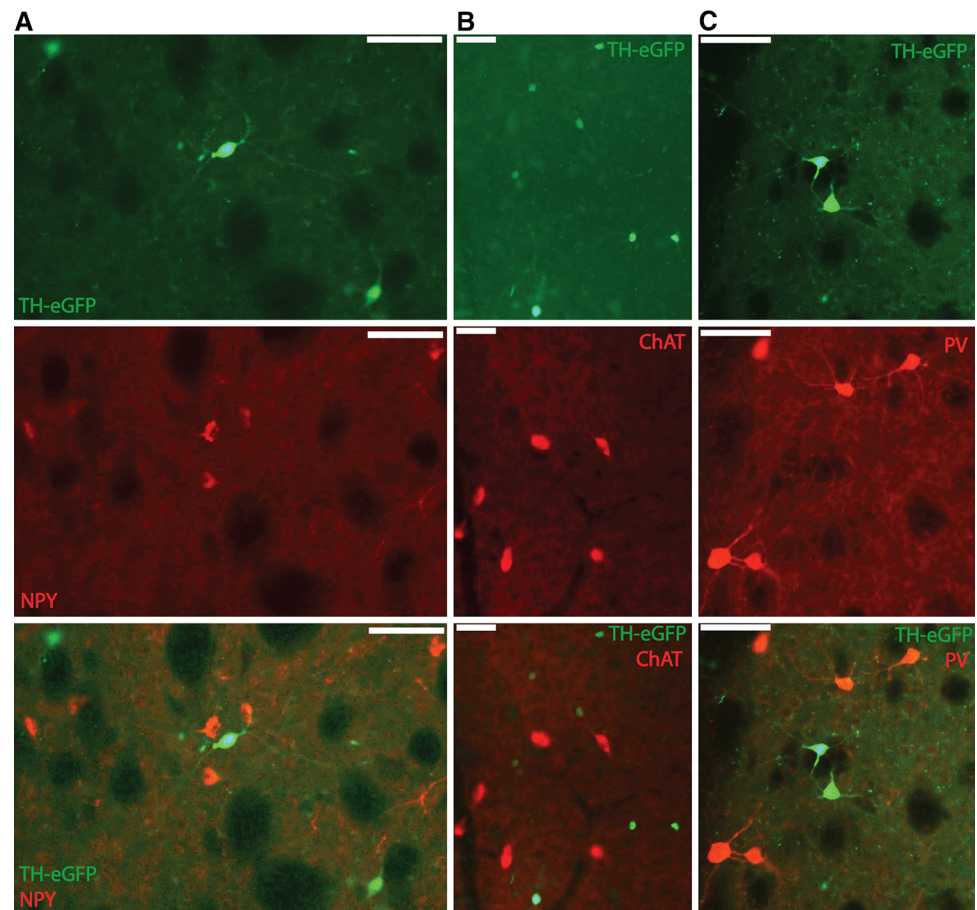
Effect of 6-OHDA lesion on intrinsic electrophysiological properties of striatal EGFP-TH interneurons

We were able to readily identify the same four electrophysiologically distinct subtypes of EGFP-TH neurons described previously in control EGFP-TH mice Ibáñez-Sandoval et al. (2010) in dopamine-denervated ($n = 75$) and vehicle-treated hemispheres ($n = 37$) in the present study. As we did not find a statistically significant difference between electrophysiological properties of dorsal and ventral striatal EGFP-TH neurons, these data were pooled.

The most frequently encountered cell type in both lesioned and vehicle-treated hemispheres (81 and 72 %, respectively) was Type I. Type I EGFP-TH interneurons exhibited a resting membrane potential around −70 mV, which is relatively more depolarized than SPNs and FSIs (Ibáñez-Sandoval et al. 2010; Koós and Tepper 1999; Wilson and Kawaguchi 1996). Although Type I EGFP-TH interneurons fire moderately accommodating action potentials near threshold, stronger depolarizing current injections result in an initial burst of action potentials with a maximal instantaneous firing rate around 45 Hz followed by a complete spike blockade, presumably due to

depolarization block. In a subpopulation of Type I interneurons, plateau potentials (PP) were observed during membrane repolarization at the offset of suprathreshold depolarizing current injection. These will be described in a separate section below. Some of the Type I interneurons showed I_h-like sag responses in response to hyperpolarizing current injections.

As reported previously (Ibáñez-Sandoval et al. 2010), some Type I EGFP-TH interneurons were found to be spontaneously active. It is interesting to note that a significantly larger proportion of Type I TH interneurons fired spontaneously in the control striatum (27.0 %, 10/37) than ipsilateral to the 6-OHDA lesion ($p < 0.05$). In addition, the mean spontaneous activity in the control striatum tended to be lower (6.11 ± 1.36 Hz) than in the lesioned striatum [4.27 ± 0.99 Hz; $t (19) = 1.14$], but this difference did not reach statistical significance; $p = 0.27$]. These data suggest that endogenous DA exerts a constitutive facilitatory effect on striatal TH interneurons.

Type II EGFP-TH interneurons comprised 6 and 10 % of EGFP-TH interneurons in 6-OHDA- and vehicle-treated striata, respectively. In stark contrast with Type I EGFP-TH neurons, Type II interneurons displayed repetitive firing in response to depolarizing current injection similar to
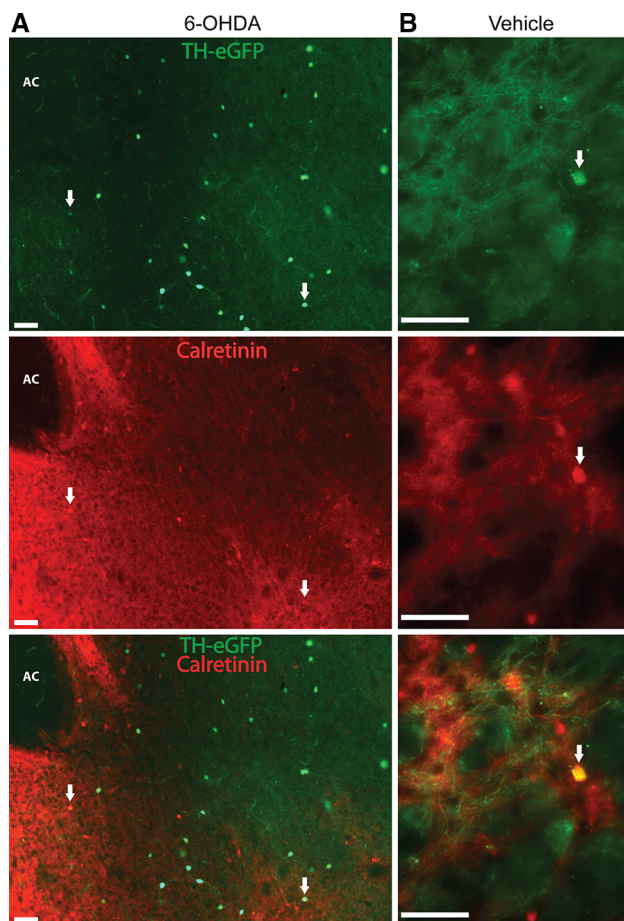
Fig. 5 Co-localization of CR immunoreactivity in a subset of EGFP-TH neurons. **a** Widefield image from 6-OHDA-treated ventral striatum. *White arrows* point to 2 EGFP-TH cells that show CR immunofluorescence. **b** CR + EGFP-TH cells were also occasionally encountered in vehicle-treated striatum. *Scale bars* 50 μm. *AC* anterior commissure

Table 1 Stereological estimates of PV, CR, NPY and ChAT-immunoreactive striatal interneurons ipsilateral to intranigral vehicle or 6-OHDA infusion

Interneuron type	Striatal population in control hemisphere (stereological estimate)	Striatal population in 6-OHDA-lesioned hemisphere (stereological estimate)
PV ($n = 4$)	13,040 ± 704	13,037 ± 593
NPY ($n = 1$)	21,486	21,473
CR ($n = 2$)	9,911 ± 854	12,192 ± 1,175
ChAT ($n = 4$)	14,090 ± 896	12,261.54 ± 1,339

Number of mice are indicated in the parentheses per given striatal interneuron marker. Mean ± SEM

that of FSIs, although the maximal firing rate of Type II EGFP-TH interneurons was around 150 Hz which is significantly slower than that in striatal PV FSIs (Koós and

Tepper 1999), and Type II EGFP-TH interneurons did not manifest depolarization block even at the highest intensities of depolarizing current pulses, as previously reported. Consistent with previous reports, Type II interneurons had a considerably lower input resistance and shorter action potential duration than Type I interneurons (Ibáñez-Sandoval et al. 2010).

Type III EGFP-TH interneurons, which were the second most prevalent cell type (14 %) in 6-OHDA-treated striatum, on the other hand, were characterized by significantly more hyperpolarized resting membrane potential, and lower input resistance. Type III interneurons exhibited the highest action potential threshold among all recorded EGFP-TH neuron types and also manifested complete spike adaptation in response to strong depolarizing current injections delivered from rest, similar to the Type I neurons.

Interestingly, Type IV neurons which were the second most commonly encountered striatal EGFP-TH interneurons in our original study (20.1 %, 29/139) were only encountered in the control hemisphere. As described previously Type IV neurons are characterized by low-threshold spiking bursts riding on a depolarization wave appearing both at the offset of hyperpolarizing pulses and in response to suprathreshold current injections (Fig. 6d). All these descriptions of the intrinsic electrophysiological properties of the EGFP-TH neurons were in good agreement with those originally reported by Ibáñez-Sandoval et al. (2010) and did not differ between control and DA-denervated striatum. The main effect of lesion did not reach statistical significance for any passive or active membrane property (Table 2) except for plateau potential and spontaneous synaptic events, described below. Typical examples of responses to current injections and the resulting IV plots for the four types of striatal EGFP-TH interneurons are shown in Fig. 6.

6-OHDA lesions of the substantia nigra altered the proportional distribution of the four EGFP-TH interneuron types [χ^2 (3) = 16.97, $p = 0.001$]. A significantly higher proportion of Type I EGFP-TH neurons was found in the DA-depleted striatum while Type IV neurons were found only in vehicle-treated striatum. These results suggest that the modest increase in the number of striatal EGFP-TH interneurons seen immediately after 6-OHDA lesions are due largely or exclusively to increases in the number of Type I interneurons, and further, that the absence of endogenous DA following destruction of the nigrostriatal pathway may promote a phenotypic shift of Type IV neurons to Type I neurons by leading to the alteration of some intrinsic ionic conductances. This latter conclusion is supported by changes in the expression of PPs described in the next section. These data along with representative biocytin fills of the four striatal EGFP-TH interneuron subtypes are shown in Fig. 6.
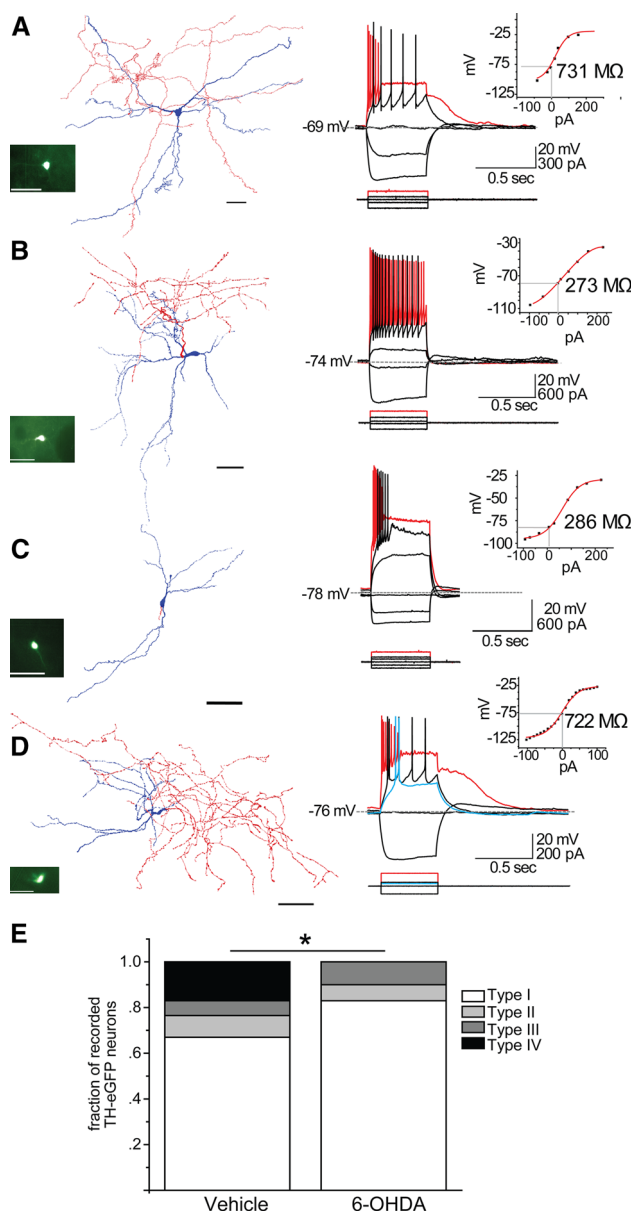
Fig. 6 Electrophysiologically identified striatal EGFP-TH subtypes across 6-OHDA and vehicle-treated hemispheres. *Left* eGFP fluorescence image of the neuron. *Middle* Neurolucida reconstructions. Soma and dendrites in *blue*, axons in *red*. *Scale bars* 50 μm. *Right* responses to 500 ms current pulses from rest. **a** Type I EGFP-TH interneuron. **b** Type II EGFP-TH interneuron. **c** Type III EGFP-TH interneuron. **d** Type IV EGFP-TH interneuron. **e** Distribution of different striatal EGFP-TH subtypes from 6-OHDA-treated and vehicle-treated hemispheres. *$*p < 0.05$ (χ^2 square test)

Effect of 6-OHDA lesion on plateau potentials in striatal EGFP-TH interneurons

There was a significant decrease in the percentage of Type I EGFP-TH neurons that expressed PP in the DA-depleted striatum (70 % in vehicle-treated STR vs. 44 % in lesioned STR, $\chi^2 = 3.625$, $p < 0.05$). Furthermore, in those cells

that expressed PPs, the plateau duration was significantly [t (37) = 2.392, $p = 0.025$] shorter ipsilateral to the nigrostriatal lesion (544 ± 62.4 ms) compared to vehicle-treated striatum (1,244 ± 291 ms) although PP amplitudes did not differ (Fig. 7). Occasionally, spontaneously generated PP (arrow) was observed to interrupt spontaneous activity, sometimes for several seconds. This only occurred in control striata. To test if the reduction in PP duration following 6-OHDA was due to the unmasking of a potassium conductance, we repeated the experiments using a Cs$^+$-based internal solution containing the membrane impermeant voltage-dependent Na$^+$ channel blocker, QX-314. Under these conditions, the same differences in PP duration between lesioned and control striata were observed. PP duration in Type I EGFP-TH interneurons from the vehicle-treated striatum were significantly [t (12) = 2.197, $p = 0.048$] longer in duration (1,765 ± 374 ms) than those ipsilateral to the 6-OHDA treatment (920 ± 185 ms) (Fig. 8). Thus, the 6-OHDA-induced decrease in PP duration is not due to the unmasking of a potassium conductance by the DA denervation.

PPs in striatal Type I EGFP-TH interneurons were highly sensitive to L-type Ca^{2+} channel blockade by bath application of 200 nM nimodipine ($n = 3$, paired t test = 5.44, $p = 0.0016$) (Fig. 8e). Taken together, these findings show that the plateau potentials in EGFP-TH neurons from DA-lesioned striatum rely on the same ionic conductances as in intact striatum (Ibáñez-Sandoval et al. 2010, 2013). L-type calcium channels activate a calcium activated non-specific cationic conductance (I$_{CAN}$) which uses Na$^+$ from TTX/QX-314-insensitive persistent sodium channels as the charge carrier (Yamashita and Isa 2003; Lee and Tepper 2007). The plateau potential appears to be a key electrophysiological characteristic in striatal EGFP-TH interneurons that is particularly sensitive to neuromodulatory regulation by endogenous DA.

Effect of 6-OHDA lesion on spontaneous synaptic currents in striatal EGFP-TH interneurons

Voltage-clamp recordings of spontaneous excitatory and inhibitory post-synaptic currents (sEPSCs and sIPSCs, respectively) were obtained using a cesium-based internal solution 1 week after unilateral 6-OHDA lesion ($n_{6\text{-OHDA}} = 14$; $n_{vehicle} = 10$), a time point where the most drastic changes in EGFP-TH cell counts were observed (see above). There was a significant increase in the frequencies of both sEPSCs and sIPSCs in EGFP-TH neurons after 6-OHDA lesion (sEPSC: 6-OHDA = 2.93 ± 0.66 Hz, vehicle = 1.20 ± 0.32 Hz; $t = 2.371$, $p = 0.033$ and sIPSC: 6-OHDA = 2.19 ± 0.37 Hz, vehicle = 1.02 ± 0.25 Hz; $t = 2.567$, $p = 0.019$), while the amplitudes (Figs. 9c, 10c) did not change (sEPSC: 6-OHDA = 16.2 ± 2.49 pA,

Table 2 Summary of the electrophysiological parameters of different subtypes of striatal EGFP-TH interneurons ipsilateral to intranigral vehicle or 6-OHDA infusion

	V_{rest} (mV)	R_{input} (MΩ)	AP threshold (mV)	AP amplitude (mV)	1st AP delay (ms)	AHP amplitude (mV)	Membrane time constant (ms)	Sag ratio	Action potential half-width (ms)	Spike frequency accommodation	Maximum firing frequency (Hz)
Type I (vehicle) n = 28	−66.22 ± 1.4	718 ± 0.7	−35.97 ± 2.9	45.7 ± 1.7	173.14 ± 28.6	16.3 ± 0.71	41.2 ± 4.4	1.03 ± 0.01	0.63 ± 0.04	1.30 ± 0.18	81.5 ± 15.2
Type I (6-OHDA) n = 58	−68.76 ± 1	641 ± 44.6	−36.11 ± 2.3	52.1 ± 1.6	177.14 ± 36	15.6 ± 0.66	33.2 ± 2.5	1.05 ± 0.06	0.56 ± 0.03	1.28 ± 0.93	96.2 ± 26.3
Type II (vehicle) n = 6	−62.36 ± 2.7	566.5 ± 63.5	−39.82 ± 0.84	56.37 ± 4.3	109.75 ± 60	14.9 ± 1.36	35.0 ± 3.94	1.03 ± 0.01	0.48 ± 0.03	1.44 ± 0.23	158.6 ± 37.5
Type II (6-OHDA) n = 4	−66.47 ± 4.2	391.4 ± 61.1	−40.1 ± 0.44	57.53 ± 6.2	77 ± 34	15.8 ± 1.2	25.47 ± 11.5	1.03 ± 0.01	0.43 ± 0.03	1.87 ± 0.42	108.8 ± 21.3
Type III (vehicle) n = 3	−73.74 ± 2.2	313.60 ± 98.0	−37.34 ± 2.4	51.67 ± 25.1	51.67 ± 25.14	16.9 ± 2.7	18.36 ± 1.0	1.02 ± 0.01	0.45 ± 0.07	1.14 ± 0.1	131.8 ± 31.97
Type III (6-OHDA) n = 10	−69.53 ± 4.0	219.77 ± 36.9	−35.01 ± 5.4	41.25 ± 18.9	41.3 ± 18.9	15.4 ± 0.93	13.65 ± 1.0	1.03 ± 0.01	0.75 ± 0.14	1.80 ± 0.4	96 ± 10.6
Type IV (vehicle) n = 7	−69.23 ± 2.9	983.24 ± 100.4	−31.31 ± 11.0	47.80 ± 4.2	144.7 ± 33.1	11.3 ± 2.61	11.27 ± 2.6	1.03 ± 0.01	0.92 ± 0.15	0.72 ± 0.1	136.5 ± 6.5
Type IV (6-OHDA) n = 0	–	–	–	–	–	–	–	–	–	–	–

Number of neurons are indicated in the parentheses per given striatal EGFP-TH subtype. Mean ± SEM
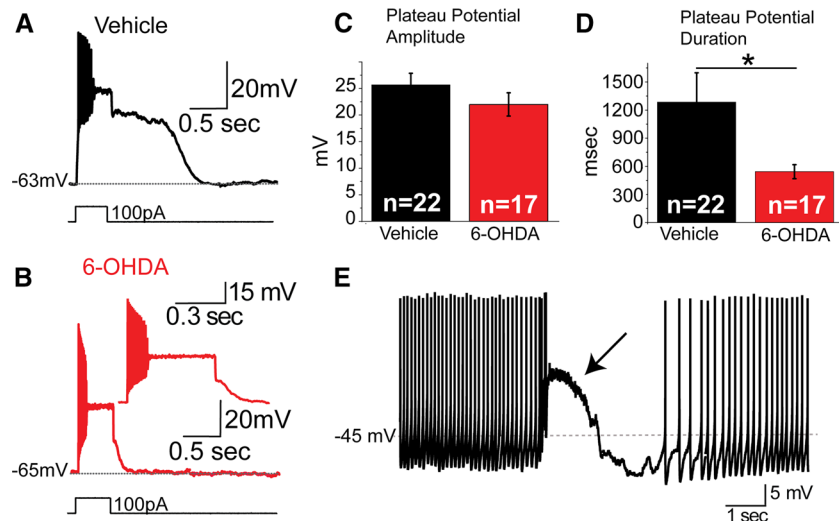
Fig. 7 Plateau potential in Type I EGFP-TH interneurons. **a** Plateau potential in a striatal Type I EGFP-TH interneuron from vehicle-treated side in response to +100 pA somatic current injection for 500 ms. **b** Plateau potential in a striatal Type I EGFP-TH neuron from 6-OHDA-treated side in response to +100 pA somatic current injection for 500 ms. *Insets* show the zoomed in view of the same neuron. **c** Plateau potentials in striatal EGFP-TH neurons from 6-OHDA- and vehicle-treated sides did not differ in terms of amplitude. **d** Plateau potentials in striatal Type I EGFP-TH neurons from 6-OHDA-treated side are significantly shorter in duration in comparison to plateau potentials in striatal Type I EGFP-TH neurons from vehicle-treated side. **e** In vehicle-treated side, in a striatal EGFP-TH subset, spontaneously generated plateau potentials (*arrow*) were also observed interrupting spontaneous firing. *$p < 0.025$ (independent *t* test)

Fig. 8 Ionic conductances underlying plateau potentials in EGFP-TH interneurons in vehicle-treated and 6-OHDA-treated striatum. Plateau potentials in EGFP-TH neurons in vehicle-treated (**a**) and 6-OHDA-treated striatum (**b**) recorded with cesium-based internal solution containing QX-314. **c** Amplitude of plateau potentials did not differ in EGFP-TH neurons between vehicle-treated and 6-OHDA-treated striatum. **d** Duration of plateau potentials in Type I EGFP-TH neurons were shorter in 6-OHDA-treated striatum as compared to vehicle treatment. *$p < 0.05$ (independent *t* test). **e** In 6-OHDA-lesioned side, plateau potential generation was highly sensitive to L-type Ca^{2+} channel antagonism by nimodipine (200 nM). *$p < 0.002$ (paired *t* test)
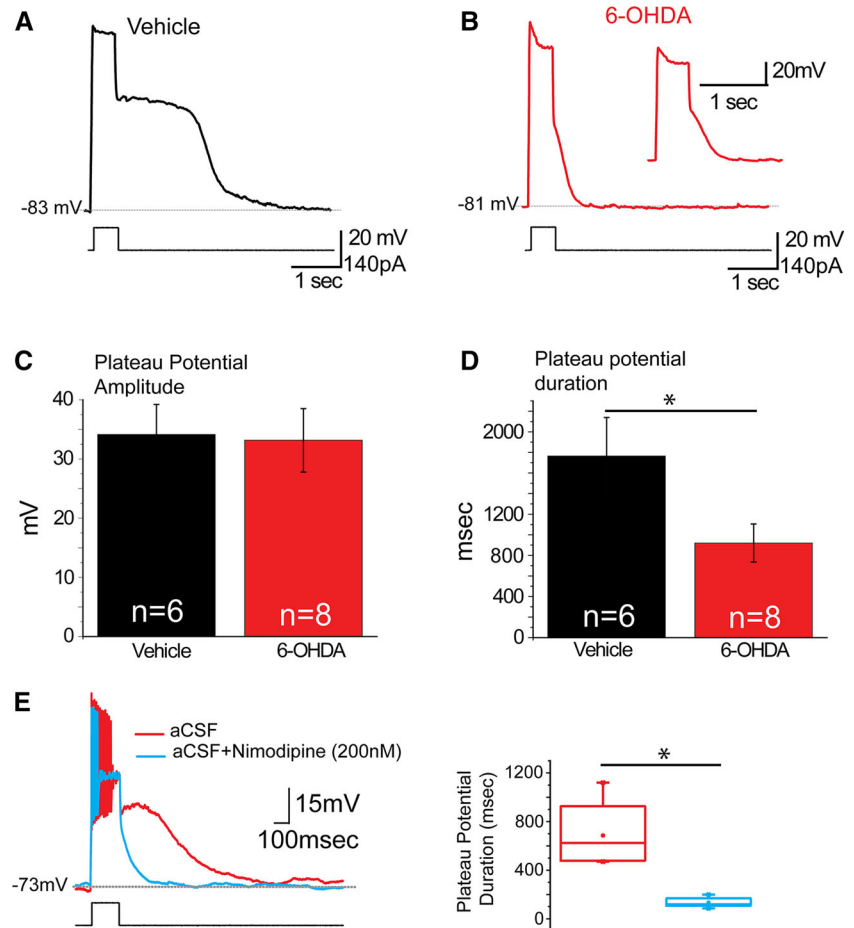
Fig. 9 Spontaneous EPSCs in striatal EGFP-TH neurons. **a** Representative current recordings from three separate cases from 1 week post-vehicle vs. 6-OHDA-treated hemispheres. *Scale bars* 10 pA, 0.5 s. **b** Frequency of spontaneous EPSCs increases significantly in striatal EGFP-TH neurons after 6-OHDA treatment. $*p < 0.05$. **c** Amplitude of spontaneous EPSCs in striatal EGFP-TH neurons do not differ in 6-OHDA-treated side. **d** Representative spontaneous EPSCs isolated from a 1 min of recording and overlay of average of spontaneous EPSCs are shown for EGFP-TH interneurons from vehicle- and 6-OHDA-treated sides. Cumulative probability plots for rise time constant (**e**), decay time constants (**f**) and inter-event intervals (**g**) of spontaneous EPSCs. Rise time constant of spontaneous EPSCs in striatal EGFP-TH neurons is significantly shorter in lesioned hemisphere (**e**). $*p < 0.05$. **g** The CV of spontaneous EPSCs in EGFP-TH neurons from 6-OHDA-treated side was significantly smaller as compared to vehicle-treated side. $*p < 0.02$
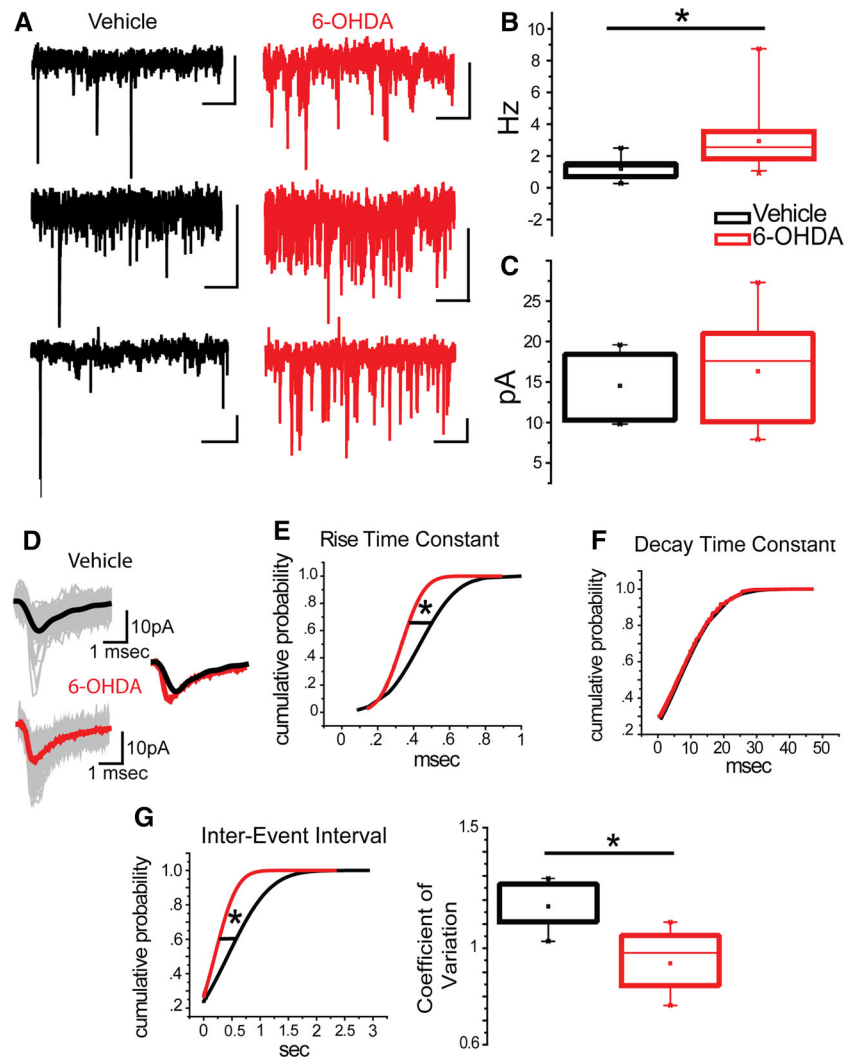
vehicle $= 14.25 \pm 2.60$ pA; $t = 0.448$, $p = 0.664$ and sIPSC: 6-OHDA $= 9.21 \pm 0.6$ pA, vehicle $= 10.04 \pm 1.3$ pA; $t = 0.392$, $p = 0.702$) (Figs. 9, 10).

The rise time constant of sEPSCs of EGFP-TH neurons ipsilateral to the 6-OHDA lesion was significantly smaller than that for the vehicle-treated hemisphere (6-OHDA $= 0.33 \pm 0.004$ ms, vehicle $= 0.44 \pm 0.01$ ms, $t_{sEPSC\ Rise} = 6.523$, $p < 0.0001$) (Fig. 9d, e). There were no significant differences between the decay time constants of sEPSCs (6-OHDA $= 6 \pm 0.62$ ms, vehicle $= 6.4 \pm 0.35$ ms, $t_{sEPSC\ Decay} = 0.580$, $p = 0.562$; Fig. 9f) or the rise (6-OHDA $= 1.17 \pm 0.05$ ms, vehicle $= 1.15 \pm 0.09$ ms, $t_{sIPSC\ Rise} = -0.136$, $p = 0.892$; Fig. 10e) or decay (6-OHDA $= 10.06 \pm 0.64$ ms, vehicle $= 10.49 \pm 1.02$ ms, $t_{sIPSC\ Decay} = 0.53$, $p = 0.958$; Fig. 10f) time constants of sIPSCs in TH-eGFPs ipsilateral to 6-OHDA treatment vs. vehicle treatment. In addition, the coefficient of variation (CV) of sEPSC inter-event intervals (IEI) (Fig. 9g), but not that of sIPSCs (Fig. 10g), in lesioned striatum was significantly smaller than in vehicle-treated striatum indicating

that there might also be changes in excitatory presynaptic inputs onto EGFP-TH neurons after striatal DA loss ($t_{CV\ of\ IEI} = 2.83$, $p = 0.017$).

Morphological changes in EGFP-TH neurons after DA depletion

Neurolucida reconstructions of 11 Type I EGFP-TH neurons from 3 days to 1 week post 6-OHDA injection were compared to eight Type I EGFP-TH neurons from vehicle-treated striatum. Representative light micrographs of Ni-DAB-reacted biocytin-filled cells and their reconstructions are shown (Fig. 11). With respect to cell bodies, measurements of EGFP-TH neurons revealed no differences in perimeter, area, aspect ratio or roundedness between lesioned and vehicle-treated striatum ($p = 0.957$; $p = 0.446$; $p = 0.498$; $p = 0.638$, respectively).

Sholl analyses were performed for dendritic arborizations by superimposing concentric spheres originating from the soma at 10 μm intervals. In terms of dendritic

arborization, MANOVA indicated the absence of significant effects of 6-OHDA lesion on dendritic length or branching ($F = 1.447$, $p = 0.233$ and $F = 0.068$, $p = 0.795$, respectively), but there was a strong effect on the density of spine-like formations on dendrites ($F = 12.038$, $p = 0.001$), particularly between 30 and 100 μm from the soma (Fig. 11).

Discussion

The present study reveals a number of anatomical, electrophysiological and morphological changes in EGFP-TH neurons after lesions of the nigrostriatal DA input. DA depletion caused a transient increase in striatal EGFP-TH cell number mainly in the ventral striatum. But even during the peak increase in EGFP-TH numbers, none of the EGFP-TH cells was found to project to striatal output structures. Furthermore, lack of immunoreactivity for PV, NPY and ChAT and marginal but unaltered overlap with

CR-expression after striatal DA loss, support the conclusion that just as in the intact striatum (Ibáñez-Sandoval et al. 2010), EGFP-TH neurons in the dopamine-depleted striatum form a distinct subtype of striatal interneurons.

Loss of the nigrostriatal DA input leads to small and transient increases in the number of striatal EGFP-TH interneurons

Previous studies that relied on immunocytochemical detection of striatal TH neurons consistently reported a many fold increase in the number of striatal TH neurons after destruction of the nigrostriatal dopaminergic pathway (Betarbet et al. 1997; Darmopil et al. 2008; Jollivet et al. 2004; Lopez-Real et al. 2003; Tandé et al. 2006). However, in the present study using BAC EGFP-TH mice and unbiased stereological cell counting, we found DA depletion only led to a 30 % overall increase in the number of EGFP-TH interneurons, and that this increase that was transient and region-specific, disappearing by the

Fig. 11 Reconstructions of striatal EGFP-TH interneurons from vehicle-treated and 6-OHDA-treated hemispheres. **a** Light micrographs of a representative Ni-DAB-reacted biocytin-filled Type I striatal EGFP-TH neuron and its reconstruction from vehicle-treated hemisphere. **b** Light micrographs of a representative Ni-DAB-reacted biocytin-filled Type I striatal EGFP-TH neuron and its reconstruction from 6-OHDA-treated hemisphere. **c** Sholl analysis on dendritic length. **d** Sholl analysis on dendritic branching. **e** Sholl analysis on dendritic spine density. Mean ± SEM (*shaded fields*). Note the increase in the density of proximal spines. *Scale bars* 50 μm (**a, b**); 10 μm (*a1–a3*); 10 μm (*b1–b3*)
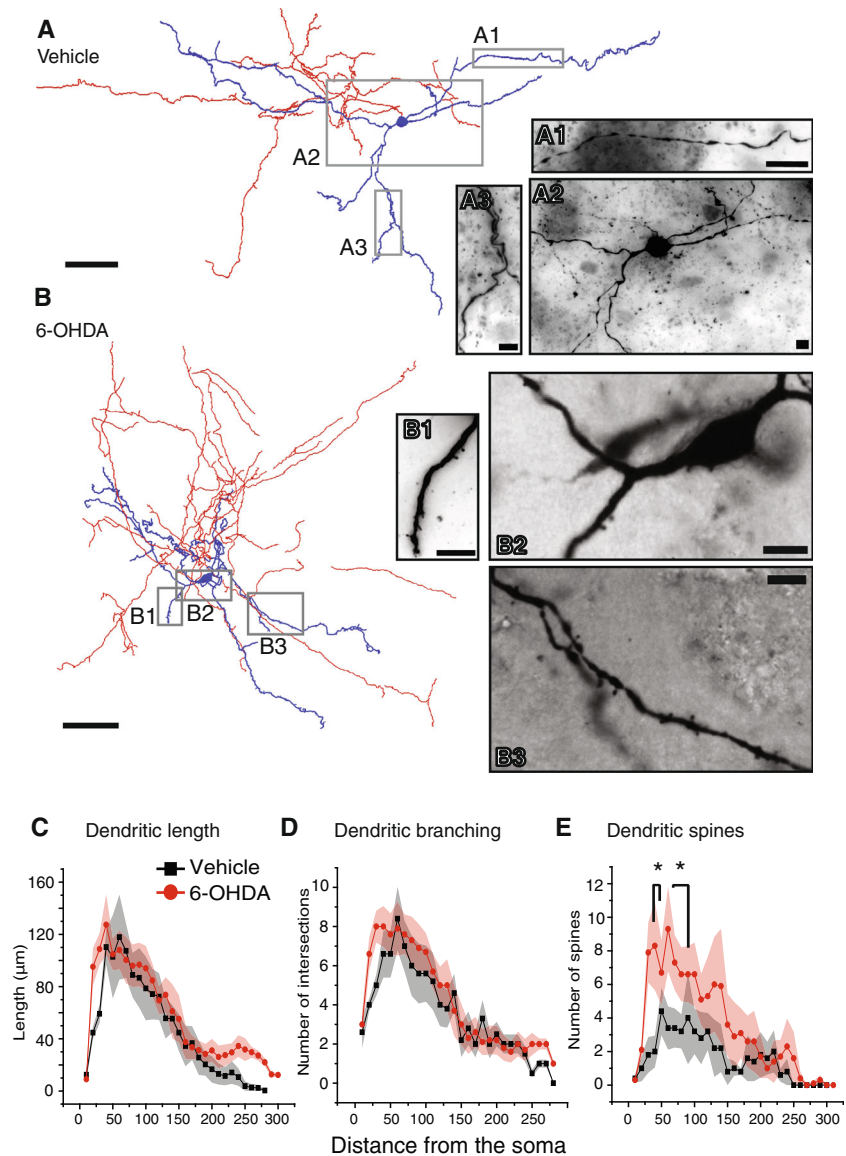
end of the second week after 6-OHDA injection into the midbrain.

In the intact striatum most EGFP-TH interneurons express very low somatic levels of TH, usually lower than detection limits by immunocytochemistry, and colchicine treatment is required to observe co-localization of TH immunofluorescence and eGFP (Ibáñez-Sandoval et al. 2010). But the transgenic EGFP reporter is a far more sensitive indicator of the presence and activity of the TH gene than is somatic immunoreactivity. This is due in part to the presence of multiple copies of the transgene coupled with its dependence on the transcriptional activity of the TH gene, not on TH levels (Gong et al. 2003). This is presumably why the baseline striatal TH cell counts reported here and previously (Ibáñez-Sandoval et al. 2010; Ünal et al. 2011) are significantly greater than those usually reported for striatal TH interneurons identified on the basis of immunocytochemistry. That the increased sensitivity of the EGFP reporter as compared to TH immunocytochemistry also accounts for the much smaller increases in cell number after lesion is supported by the observation that DA denervation leads to increases in TH transcriptional activity and TH levels and thereby increases the proportion of EGFP-TH interneurons that also reveal TH immunofluorescence (c.f. Fig. 1). Thus, when using TH immunocytochemistry for identification of striatal TH interneurons, the DA denervation has the effect of increasing the somatic levels of TH from a level below the limits of immunocytochemical detectability to one where TH immunocytochemistry can now detect them. In the EGFP-TH mice, however, the striatal TH neurons that express very low levels of TH are already visible due to the increased sensitivity of the EGFP reporter. Thus, the majority of the apparently "newly appearing" or "increased" number of

TH immunoreactive neurons in interneurons after 6-OHDA lesion are already visible in the EGFP-TH mice prior to the lesion. The neurons were always there, they just could not be detected with TH immunocytochemistry.

Regional variation in changes in the number of striatal TH interneurons after 6-OHDA lesions

The majority of the modest increase in the number of EGFP-TH interneurons after 6-OHDA lesions happens in the ventral striatum soon after the lesion and is transient. This is somewhat surprising given that ventral striatum receives DA input primarily from the VTA, and that region was largely spared in our mice. Previous studies indicate that striatal TH neurons may exhibit an intimate relationship with nigrostriatal DA input. Busceti et al. (2008, 2012) have shown that immunoreactive striatal TH somata are abundant between postnatal days (PD) 1–8, at a time when the dopaminergic innervation is patchy. The number of TH neurons declines between PD 8–16 when the second wave of dopaminergic innervation starts targeting the entire striatum. In addition, following intrastriatal 6-OHDA, Darmopil et al. (2008) detected the "emergence" of TH immunoreactive neurons only in domains that had surviving dopaminergic fibers, but not in striatal areas that underwent a complete dopamine fiber loss. However, it should be noted that these neurons are spiny projection neurons, and not the striatal TH interneurons that are the subject of the present experiments. It was hypothesized earlier that surviving dopaminergic fibers may exert trophic effects (Huot and Parent 2007) in the striatum. Indeed, local growth factors in MPTP-treated monkeys potentiate the "increase" in the numbers of striatal TH neurons (Palfi et al. 2002; San Sebastián et al. 2007) and can be released by dopaminergic neurons (Bustos et al. 2004). Although striatal TH interneurons appear to increase in the earlier stages of PD when there is still some dopaminergic innervation of striatum (Porritt et al. 2000), they disappear in later stages when DA levels are severely compromised (Porritt et al. 2006). Perhaps something similar is happening in the EGFP-TH mice.

Electrophysiological changes in striatal EGFP-TH neurons after 6-OHDA lesion

The relative abundance of the different EGFP-TH subtypes differed between 6-OHDA and vehicle conditions. Low-threshold spiking Type IV neurons that make up $\sim$20 to 25 % of EGFP-TH population in the intact striatum Ibáñez-Sandoval et al. (2010) were absent following unilateral intranigral 6-OHDA at all 4 time points investigated. Parallel to this, we found that Type I neurons made up of $\sim$80 % of the electrophysiologically identified cells in the lesioned hemisphere, but only about 64 % of the

population in the vehicle-treated side. The Type I cell proportion on the vehicle-treated side is the same as that originally reported for naïve EGFP-TH mice (60.4 %, 84/139; Ibáñez-Sandoval et al. 2010). These findings suggest the possibility of a phenotypic conversion within the EGFP-TH interneuronal population from Type IV to Type I, as a result of sustained DA loss. It is also possible that unlike the other striatal TH interneurons, Type IV neurons may be susceptible to the neurotoxic effects of 6-OHDA and the increase in Type I neurons reflects their greater baseline proportion of all striatal TH interneurons.

Other than the shift in proportional distribution of the striatal EGFP-TH interneuron subtypes described above, there were little or no changes in their intrinsic electrophysiological properties except for those relating to PPs after 6-OHDA lesion. We found a significant reduction in the proportion of EGFP-TH neurons that expressed PPs and in those EGFP-TH neurons that did express PPs, their duration was significantly shorter in the DA-depleted side. To unmask the possible involvement of voltage-gated potassium conductance that might suppress the PP as a source for the reduction in plateau potentials after DA loss, whole cell recordings of EGFP-TH neurons were obtained with a cesium-based internal solution containing QX-314. In these recordings, the reduction in PP duration after DA depletion persisted, eliminating the possibility of an unmasked potassium conductance. Just as in the intact striatum, the PP after DA loss was highly sensitive to an L-type calcium channel antagonist. As in the intact striatum Ibáñez-Sandoval et al. (2010), this suggests that the PPs are triggered by Ca^{2+} influx through L-type channels which in turn activate I_{CAN} that uses Na^+ influx from persistent Na^+ channels as the charge carrier, reminiscent of the plateau generation mechanism in the substantia nigra (Yamashita and Isa 2003; Lee and Tepper 2007). The PPs in EGFP-TH neurons are potentiated by bath application of amphetamine, DA and the selective D1/D5 agonist, SK38393 Ibáñez-Sandoval et al. (2010 and unpublished observations) supporting the present findings that the ionic conductances underlying the PPs are strongly modulated by endogenous DA and are thus down-regulated after DA loss.

There were significant increases in the frequency of sEPSCs and sIPSCs in EGFP-TH interneurons and a significant reduction in the rise time constant of sEPSCs 1 week after 6-OHDA lesion. Concomitantly, we found a significant increase in the number of dendritic spine-like formations on proximal dendrites. Thus, the alteration of the kinetics of sEPSCs in EGFP-TH interneurons after dopamine depletion may be the result of additional EPSCs being generated at more proximal dendritic regions with a consequent reduction in their electrotonic attenuation (e.g., Maccaferri et al. 2000; Gustafson et al. 2006).

There is evidence for increase in excitatory drive in the DA-depleted striatum, such as over coupling to cortical slow rhythm and heightened firing during up-states in SPNs in anesthetized in vivo preparations (Tseng et al. 2001), and an increased frequency of depolarizing synaptic potentials (Calabresi et al. 2000) in vitro. The significant reduction in the CV of excitatory events suggests a presynaptic change in excitatory drive after DA depletion. In a recent in vivo study using freely moving rats that had been unilaterally DA lesioned, Dejean et al. (2012) demonstrated a significant increase in high-voltage spindle activity originating from the cortex and increased coherence in the 5–13 Hz band between cortex and striatum emerging around 1 week post-lesion. Structurally, an increased prevalence of vesicular glutamate transporter 1-expressing cortical terminals has been noted in the striatum of MPTP-treated monkeys (Raju et al. 2008). This heightened excitatory drive not only targets SPNs but also striatal interneuronal circuitry. Dehorter et al. (2009) showed heightened oscillatory activity in LTS-type GABAergic interneurons after DA loss. Recently, Gittis et al. (2011) found that the probability of synaptic connections between FSIs and striatopallidal SPNs increased after 6-OHDA, which was accompanied by a dramatic sprouting of the axonal arborization of the FSIs. In addition, the absence of striatal DA also increases cholinergic interneuron excitability (Fino et al. 2007; Zackheim and Abercrombie 2005), which could lead to increased feedforward inhibition of SPNs through recently described nicotinic-dependent GABAergic mechanisms (Ibáñez-Sandoval et al. 2010, 2011; English et al. 2011). Thus, increases in cortical drive and feedforward inhibition in the striatum and cholinergic activation (Luo et al. 2012) after DA loss are likely responsible, at least in part, for the changes we saw in sIPSC and sEPSCs in EGFP-TH interneurons.

Functional considerations

When they were first discovered, and found to greatly increase in number following destruction of the nigrostriatal dopaminergic pathway, striatal TH interneurons were assumed to be dopaminergic and to increase in number to help compensate the DA-denervated striatum by supplying an intrinsic source of DA (e.g., Betarbet et al. 1997; Porritt et al. 2000; Huot and Parent 2007). However, recent findings have revealed that striatal TH interneurons are GABAergic (Ibáñez-Sandoval et al. 2010) not dopaminergic, and cannot be induced to release measurable quantities of DA (Xenias et al. 2012, unpublished data). What then might be the significance of the changes in their number, morphology and physiology following 6-OHDA lesions of the substantia nigra? Even though they cannot not serve as

a source of DA to compensate for the loss of the nigrostriatal pathway (Xenias et al. 2012; unpublished data), the striatal TH interneurons are well integrated into the synaptic circuitry of the striatum and may still help compensate for the loss of striatal DA by increasing feedforward GABAergic inhibition of SPNs (Ibáñez-Sandoval et al. 2010) and countering the hyperactivity that occurs in indirect pathway SPNs in experimental and idiopathic Parkinson's disease (Schultz and Ungerstedt 1978; Kita and Kita 2011).

References

Betarbet R, Turner R, Chockkan V, DeLong MR, Allers KA, Walters J, Levey AI, Greenamyre JT (1997) Dopaminergic neurons intrinsic to the primate striatum. J Neurosci 17:6761–6768

Breese GR, Traylor TD (1971) Depletion of brain noradrenaline and dopamine by 6-hydroxydopamine. Br J Pharmacol 42:88–99

Busceti CL, Biagioni F, Mastroiacovo F, Bucci D, Lenzi P, Pasquali L, Trabucco A, Nicoletti F, Fornai F (2008) High number of striatal dopaminergic neurons during early postnatal development: correlation analysis with dopaminergic fibers. J Neural Transm 115:1375–1383

Busceti CL, Bucci D, Molinaro G, Di Pietro P, Zangrandi L, Gradini R, Moratalla R, Battaglia G, Bruno V, Nicoletti F, Fornai F (2012) Lack or inhibition of dopaminergic stimulation induces a development increase of striatal tyrosine hydroxylase-positive interneurons. PLoS One 7(9):e44025

Bustos G, Abarca J, Campusano J, Bustos V, Noriega V, Aliaga E (2004) Functional interactions between somatodendritic dopamine release, glutamate receptors and brain-derived neurotrophic factor expression in mesencephalic structures of the brain. Brain Res Brain Res Rev 47:126–144

Calabresi P, Centonze D, Bernardi G (2000) Electrophysiology of dopamine in normal and denervated striatal neurons. Trends Neurosci 23:S57–S63

Cenci MA, Lundblad M (2007) Ratings of L-DOPA-induced dyskinesia in the unilateral 6-OHDA lesion model of Parkinson's disease in rats and mice. Curr Protoc Neurosci Chapter 9:Unit 9.25

Darmopil S, Muñetón-Gómez VC, de Ceballos ML, Bernson M, Moratalla R (2008) Tyrosine hydroxylase cells appearing in the mouse striatum after dopamine denervation are likely to be projection neurones regulated by L-DOPA. Eur J Neurosci 27:580–592

Dehorter N, Guigoni C, Lopez C, Hirsch J, Eusebio A, Ben-Ari Y, Hammond C (2009) Dopamine-deprived striatal GABAergic interneurons burst and generate repetitive gigantic IPSCs in medium spiny neurons. J Neurosci 29:7776–7787

Dejean C, Nadjar A, Le Moine C, Bioulac B, Gross CE, Boraud T (2012) Evolution of the dynamic properties of the cortex-basal ganglia network after dopaminergic depletion in rats. Neurobiol Dis 46:402–413

Dubach M, Schmidt R, Kunkel D, Bowden DM, Martin R, German DC (1987) Primate neostriatal neurons containing tyrosine hydroxylase: immunohistochemical evidence. Neurosci Lett 75:205–210

English DF, Ibáñez-Sandoval O, Stark E, Tecuapetla F, Buzsaki G, Deisseroth K, Tepper JM, Koós T (2011) GABAergic circuits mediate the reinforcement-related signals of striatal cholinergic interneurons. Nat Neurosci 15:123–130

Fino E, Glowinski J, Venance L (2007) Effects of acute dopamine depletion on the electrophysiological properties of striatal neurons. Neurosci Res 58:305–316

Franklin KBJ, Paxinos G (2007) The mouse brain in stereotaxic coordinates, 3rd edn. Academic Press, San Diego

Gittis AH, Nelson AB, Thwin MT, Palop JJ, Kreitzer AC (2010) Distinct roles of GABAergic interneuron in the regulation of striatal output pathways. J Neurosci 30:2223–2234

Gittis AH, Hang GB, LaDow ES, Shoenfeld LR, Atallah BV, Finkbeiner S, Kreitzer AC (2011) Rapid target-specific remodeling of fast-spiking inhibitory circuits after loss of dopamine. Neuron 71:858–868

Gong S, Zheng C, Doughty ML, Losos K, Didkovsky N, Schambra UB, Nowak NJ, Joyner A, Leblanc G, Hatten ME, Heintz N (2003) A gene expression atlas of the central nervous system based on bacterial artificial chromosomes. Nature 425:917–925

Gustafson N, Gireesh-Dharmaraj E, Czubayko U, Blackwell KT, Plenz D (2006) A comparative voltage and current-clamp analysis of feedback and feedforward synaptic transmission in the striatal microcircuit in vitro. J Neurophysiol 95:737–752

Henny P, Brown MT, Northrop A, Faunes M, Ungless MA, Magill PJ, Bolam JP (2012) Structural correlates of heterogeneous in vivo activity of midbrain dopaminergic neurons. Nat Neurosci 15:613–619

Huot P, Parent A (2007) Dopaminergic neurons intrinsic to the striatum. J Neurochem 101:1441–1447

Huot P, Levesque M, Parent A (2007) The fate of striatal dopaminergic neurons in Parkinson's disease and Huntington's chorea. Brain 130:222–232

Ibanez-Sandoval O, Tecuapetla F, Unal B, Shah F, Koos T, Tepper JM (2011) A novel functionally distinct subtype of striatal neuropeptide Y interneuron. J Neurosci 31:16757–16769

Ibáñez-Sandoval O, Tecuapetla F, Ünal B, Shah F, Koós T, Tepper JM (2010) Electrophysiological and morphological characteristics and synaptic connectivity of tyrosine hydroxylase-expressing neurons in adult mouse striatum. J Neurosci 30:6999–7016

Jollivet C, Montero-Menei CN, Venier-Julienne MC, Sapin A, Benoit JP, Menei P (2004) Striatal tyrosine hydroxylase immunoreactive neurons are induced by L-dihydroxyphenylalanine and nerve growth factor treatment in 6-hydroxydopamine lesioned rats. Neurosci Lett 362:79–82

Kawaguchi Y (1993) Physiological, morphological and histochemical characterisation of three classes of interneurons in the neostriatum. J Neurosci 13:4908–4923

Kawaguchi Y (1997) Neostriatal cell subtypes and their functional roles. Neurosci Res 27:1–8

Kita H, Kita T (2011) Cortical stimulation evokes abnormal responses in the dopamine-depleted rat basal ganglia. J Neurosci 31:10311–10322

Koós T, Tepper JM (1999) Inhibitory control of neostriatal projection neurons by GABAergic interneurons. Nat Neurosci 2:467–472

Koós T, Tepper JM, Wilson CJ (2004) Comparison of IPSCs evoked by spiny and fast-spiking neurons in the neostriatum. J Neurosci 24:7916–7922

Lee CR, Tepper JM (2007) A calcium-activated nonselective cation conductance underlies the plateau potential in rat substantia nigra GABAergic neurons. J Neurosci 27:6531–6541

Lopez-Real A, Rodriguez-Pallares J, Guerra MH, Labandeira-Garcia JL (2003) Localization and functional significance of striatal neurons immunoreactive to aromatic L-amino acid decarboxylase or tyrosine hydroxylase in rat parkinsonian models. Brain Res 969:135–146

Luo R, Schroeder MJ, Partridge JG, Vicini S (2012) Direct and GABA mediated indirect effects of nicotinic ACh receptor agonists on striatal neurones. J Physiol 591:203–207

Maccaferri G, Roberts JD, Szucs P, Cottingham CA, Somogyi P (2000) Cell surface domain specific postsynaptic currents evoked by identified GABAergic neurones in rat hippocampus in vitro. J Physiol 524(1):91–116

Masuda M, Miura M, Inoue R, Imanishi M, Saino-Saito S, Takada M, Kobayashi K, Aosaki T (2011) Postnatal development of tyrosine hydroxylase mRNA-expressing in mouse neostriatum. Eur J Neurosci 34(9):1355–1367

Mathus BN, Capik NA, Alvarez VA, Lovinger DM (2011) Serotonin induces long-term depression at corticostriatal synapses. J Neurosci 31(20):7402–7411

Mazloom M, Smith Y (2006) Synaptic microcircuitry of tyrosine hydroxylase-containing neurons and terminals in the striatum of 1-methyl-4-phenyl-1,2,3,6-tetrahydropyridine treated monkeys. J Comp Neurol 495:453–469

Meredith GE, Farrell T, Kellaghan P, Tan Y, Zahm DS, Toterdell S (1999) Immunocytochemical characterization of catecholaminergic neurons in the rat striatum following dopamine-depleting lesions. Eur J Neurosci 11:3583–3596

Palfi S, Leventhal L, Chu Y, Ma SY, Emborg M, Bakay R, Deglon N, Hantraye P, Aebischer P, Kordower JH (2002) Lentivirally delivered glial cell line-derived neurotrophic factor increases the number of striatal dopaminergic neurons in primate models of nigrostriatal degeneration. J Neurosci 22:4942–4954

Porritt MJ, Batchelor PE, Hughes AJ, Kalnins R, Donnan GA, Howells DW (2000) New dopaminergic neurons in Parkinson's disease striatum. Lancet 356:44–45

Porritt MJ, Kingsbury AE, Hughes AJ, Howells DW (2006) Striatal dopaminergic neurons are lost with Parkinson's disease progression. Mov Disord 21:2208–2211

Raju DV, Ahem TH, Wright TM, Standaert DG, Hall RA, Smith Y (2008) Differential synaptic plasticity of the corticostriatal and thalamostriatal systems in an MPTP-treated monkey model of Parkinsonism. Eur J Neurosci 27:1647–1658

Rymar VV, Sasseville R, Luk KC, Sadikot AF (2004) Neurogenesis and stereological morphometry of calretinin immunoreactive GABAergic interneurons of the neostriatum. J Comp Neurol 469:325–339

San Sebastián W, Guillén J, Manrique M, Belzunegui S, Ciordia E, Izal-Azcárate A, Garrido-Gil P, Vázquez-Claverie M, Luquin MR (2007) Modification of the number and phenotype of striatal dopaminergic cells by carotid body graft. Brain 130:1306–1316

Schultz W, Ungerstedt U (1978) Short-term increase and long-term reversion of striatal cell activity after degeneration of the nigrostriatal dopamine system. Exp Brain Res 33:159–171

Sholl DA (1953) Dendritic organization in the neurons of the visual and motor cortices of the cat. J Anat 87(4):387–406

Tandé D, Hoglinger G, Debeir T, Freundlieb N, Hirsch EC, Francois C (2006) New striatal dopamine neurons in MPTP-treated macaques result from a phenotypic shift and not neurogenesis. Brain 129:1194–1200

Tashiro Y, Sugimoto T, Hattori T, Uemura Y, Nagatsu I, Kikuchi H, Mizuno N (1989) Tyrosine hydroxylase-like immunoreactive neurons in the striatum of the rat. Neurosci Lett 97:6–10

Tepper JM, Bolam JP (2004) Functional diversity and specificity of neostriatal interneurons. Curr Opin Neurobiol 14:685–692

Tepper JM, Tecuapetla F, Koós T, Ibáñez-Sandoval O (2010) Heterogeneity and diversity of striatal GABAergic interneurons. Front Neuroanat 4:150. doi:10.3389/fnana.2010.00150

Tseng KY, Kasanetz F, Kargieman L, Riquelme LA, Murer MG (2001) Cortical slow oscillatory activity is reflected in the membrane potential and spike trains of striatal neurons in rats with chronic nigrostriatal lesions. J Neurosci 21:6430–6439

Ugrumov MV (2009) Non-dopaminergic neurons partly expressing dopaminergic phenotype: distribution in the brain, development and functional significance. J Chem Neuroanat 38:241–256

Ünal B, Ibáñez-Sandoval O, Shah F, Abercrombie ED, Tepper JM (2011) Distribution of tyrosine hydroxylase-expressing interneurons with respect to anatomical organization of the neostriatum. Front Syst Neurosci 5:41

Ungless MA, Magill PJ, Bolam JP (2004) Uniform inhibition of dopamine neurons in the ventral tegmental area by aversive stimuli. Science 303:2040–2042

Wilson CJ, Kawaguchi Y (1996) The origins of two-state spontaneous membrane potential fluctuations of neostriatal spiny neurons. J Neurosci 16:2397–2410

Wu Y, Parent A (2000) Striatal interneurons expressing calretinin, parvalbumin and NADPH-diaphorase: a comparative study in the rat, monkey and human. Brain Res 863:182–191

Xenias H, Shah F, Koós T, Tepper JM (2012) Voltammetric studies of dopamine release from optogenetically activated striatal TH+ interneurons. Soc Neurosci Abstr 183.12/LL3

Yamashita T, Isa T (2003) Flufenamic acid sensitive, Ca(2+)-dependent inward current induced by nicotinic acetylcholine receptors in dopamine neurons. Neurosci Res 46:463–473

Zackheim J, Abercrombie ED (2005) Thalamic regulation of striatal acetylcholine efflux is both direct and indirect and qualitatively altered in the dopamine-depleted striatum. Neuroscience 131: 423–436